Detection of Secondary Thalamic Degeneration After Cortical Infarction Using *cis*-4-^{18}F-Fluoro-D-Proline

Karl-Josef Langen[1,2], Dagmar Salber[3], Kurt Hamacher[2,4], Gabriele Stoffels[3], Guido Reifenberger[5], Dirk Pauleit[1,2], Heinz H. Coenen[3,4], and Karl Zilles[1–3]

[1]Institute of Neuroscience and Biophysics–Medicine, Research Centre Jülich, Jülich, Germany; [2]Brain Imaging Centre West, Research Centre Jülich, Jülich, Germany; [3]C. & O. Vogt Institute of Brain Research, Heinrich-Heine-University, Düsseldorf, Germany; [4]Institute of Neuroscience and Biophysics–Nuclear Chemistry, Research Centre Jülich, Jülich, Germany; and [5]Department of Neuropathology, Heinrich-Heine-University, Düsseldorf, Germany

The amino acid *cis*-4-^{18}F-fluoro-D-proline (D-*cis*-^{18}F-FPro) exhibits preferential uptake in the brain compared with its L-isomer, but the clinical potential of the tracer is as yet unkown. In this study we explored the cerebral uptake of D-*cis*-^{18}F-FPro in rats with focal cortical infarctions. **Methods:** Focal cortical infarctions were induced in different areas of the cortex of 20 Fisher CDF rats by photothrombosis (PT). At variable time points after PT (1 d to 4 wk), the rats were injected intravenously with D-*cis*-^{18}F-FPro. For comparison, 12 rats were injected simultaneously with ^{3}H-deoxyglucose (^{3}H-DG), 3 rats were injected with ^{3}H-*methyl*-L-methionine (^{3}H-MET), and 2 rats were injected with ^{3}H-PK11195. Within 2 h after injection of the tracers, coronal cryosections of the brains were produced and evaluated by dual-tracer autoradiography. Lesion-to-brain ratios (L/B ratios) were calculated by dividing the maximal uptake in areas with increased tracer uptake by the mean uptake in normal brain tissue. Histologic slices were stained by toluidine blue and by immunostainings for glial fibrillary acidic protein (GFAP), CD68 for macrophages, and CD11b for microglia. **Results:** Prominent uptake of D-*cis*-^{18}F-FPro was found in ipsilateral thalamic nuclei (TN) and partially in the corpus striatum starting at 3 d after infarction with increasing L/B ratios up to 4 wk (mean L/B ratio ± SD, 6.7 ± 3.5). The involved TN varied with the site of the cortical lesion corresponding to their thalamocortical projections connecting them with their specific target region in the cerebral cortex. The TN were positive for CD11b and GFAP from day 7 onward, whereas uptake of ^{3}H-DG, ^{3}H-MET, and ^{3}H-PK11195 and immunostaining for CD68 were similar to that of normal brain. Furthermore, increased uptake of D-*cis*-^{18}F-FPro was found in the area of the cortical infarctions (mean L/B ratio ± SD, 12.1 ± 8.1). From day 5 onward, the pattern of uptake was congruent with that of immunostaining for CD11b and CD68 but was different from that of GFAP. **Conclusion:** D-*cis*-^{18}F-FPro appears to be a sensitive PET tracer for detection of secondary degeneration of TN after cortical injury. The uptake mechanisms of D-*cis*-^{18}F-FPro remain to be elucidated, but the relationship to microglial activation suggests a diagnostic potential in various brain diseases.

Key Words: *cis*-4-^{18}F-fluoro-D-proline; cortical infarction; thalamic degeneration; PET; microglia

J Nucl Med 2007; 48:1482–1491
DOI: 10.2967/jnumed.107.041699

Amino acids play an important role in virtually all biologic processes. These substrates serve not only as basic modules of proteins and hormones but also as neurotransmitters, synaptic modulators, and neurotransmitter precursors. In the brain, L-proline has been shown to act as a modulator of excitatory neurotransmission (*1*), a process that is disturbed in many brain diseases such as ischemia, trauma, and gliomas (*2*).

cis-4-^{18}F-Fluoro-L-proline (L-*cis*-^{18}F-FPro) has been considered as a PET tracer for tumor imaging (*3,4*) but initial results in peripheral tumors were disappointing (*5*). In brain tumors, some uptake was found in areas with disruption of the blood–brain barrier (BBB) but uptake of L-*cis*-^{18}F-FPro in the normal brain was poor (*6*).

Recently, we observed that the D-isomer of *cis*-^{18}F-FPro is transported across the BBB in contrast to L-*cis*-^{18}F-FPro (*7*). Similar to this finding, an intensive labeling of the cerebral cortex has been reported after injection of D-^{3}H-proline in mice, whereas cortical uptake of L-^{3}H-proline was negligible (*8*). The radioactivity in the brain after injection of D-^{3}H-proline was due to L-^{3}H-proline, indicating the existence of a proline racemase in the brain converting D-proline to L-proline (*9,10*).

To explore the diagnostic potential of D-*cis*-^{18}F-FPro in vascular disorders we investigated the uptake of the tracer after cerebral ischemia in rats. Transient and permanent occlusion of the middle cerebral artery has been widely used to induce ischemic brain lesions. However, the lesions induced by this technique are variable in size, and a reliable

Received Mar. 13, 2007; revision accepted May 16, 2007.
For correspondence or reprints contact: Karl-Josef Langen, MD, Institute of Neuroscience and Biophysics–Medicine, Research Centre Jülich, D-52425 Jülich, Germany.
E-mail: k.j.langen@fz-juelich.de

distinction between the ischemic lesion, the border zone, and remote areas in the brain, which are not directly affected by ischemia, is almost impossible. The photothrombosis (PT) model using the photosensitive dye rose bengal (Sigma Aldrich Chemie GmbH) induces small, topographically defined lesions within the cerebral cortex (*11*). These focal lesions cause functional and structural changes throughout the brain during the initial phase as well as during postlesional degeneration and regeneration (*12*). In initial experiments, we observed increased uptake of D-*cis*-^{18}F-FPro in the area of the cortical infarction but also remarkable uptake in ipsilateral thalamic nuclei (TN). To further explore this phenomenon we induced focal infarctions in different cortical areas and at different time points after PT. In addition, D-*cis*-^{18}F-FPro uptake was compared with that of D-^{3}H-deoxyglucose (DG) and ^{3}H-methyl-L-methionine (L-MET) as well as with ^{3}H-PK11195, a ligand for peripheral benzodiazepine receptors, which has been shown to accumulate in TN after cortical infarctions (*13,14*). The corresponding histologic slices were analyzed by immunofluorescent imaging using various markers to investigate the cellular components involved in the uptake process of D-*cis*-^{18}F-FPro.

MATERIALS AND METHODS

Radiotracers

D-*cis*-^{18}F-FPro was prepared via cryptate mediated n.c.a. nucleophilic ^{18}F-fluorination starting from (2*R*,4*S*)-*N*-Boc-4-(*p*-toluolsulfonyloxy)proline methylester. *N*-Deprotection and ester hydrolysis took place under acidic conditions in the presence of aqueous trifluoromethanesulfonic acid. High-performance liquid chromatography purification combined with online solid-phase extraction yielded the diastereomerically pure D-*cis*-^{18}F-FPro, with a radiochemical yield of about 30% within 90 min, a radiochemical purity of >98%, and a specific radioactivity of >150 TBq/mmol.

D-^{3}H-Deoxyglucose (^{3}H-DG) with a specific radioactivity of 300 GBq/mmol (Amersham Biosciences Europe GmbH), ^{3}H-PK11195 with a specific radioactivity of 2.6 TBq/mmol (Perkin Elmer LAS GmbH), and ^{3}H-*methyl*-L-methionine (^{3}H-MET) with a specific radioactivity of 3 TBq/mmol (Amersham Biosciences Europe GmbH) were obtained commercially.

Animals

Twenty male Fisher CDF rats (8- to 12-wk old; weight, 250–300 g; Charles River Wiga) were examined in this study. The experiments were approved by the district government according to the German Law on the Protection of Animals (Cologne/Germany no. 50.203.2-KFA 5/03).

The animals were maintained under standard conditions with free access to food and water. Circumscribed cortical infarctions were generated using the PT model (*11*). In brief, animals were sedated in an isoflurane atmosphere (2%–5%) and anesthetized with an intraperitoneal injection of ketamine (100 mg/kg)/xylazine (10 mg/kg). After the animals had been placed in a stereotactic frame, focal lesions were produced in the cerebral cortex. The skin of the skull was incised and an optical fiber bundle, mounted onto a cold light source (KL1500 LCDZeiss), was placed on the skull.

According to a stereotactic brain atlas (*15*), the light source was positioned at different sites to induce infarctions in variable cortical areas: (i) 2 mm anterior to the bregma and 2 mm lateral to the midline to induce infarctions in the motor cortex, (ii) 2 mm posterior to the bregma and 3 mm lateral to the midline to induce infarctions in the somatosensory cortex, and (iii) 7 mm posterior to the bregma and 3 mm lateral to the midline to induce infarctions in the visual cortex.

Thereafter, 1.3 mg rose bengal/100 g body weight was injected intravenously and, shortly thereafter, the light was turned on for 20 min. After illumination, the catheter and light source were removed and the incision was sutured. The treatment produced cortical infarctions of variable sizes with a mean diameter ± SD of 5.3 ± 1.8 mm.

Autoradiography

At variable time points (1 d to 4 wk) after induction of the PT (Table 1), animals were anesthesized again for tracer injection via the jugular vein. All animals were injected with 80 MBq D-*cis*-^{18}F-FPro. One hour later, 12 animals received 10 MBq ^{3}H-DG as a second injection, 3 animals received 5 MBq ^{3}H-L-MET, and 2 animals received 5 MBq ^{3}H-PK11195 at 105 min after D-*cis*-^{18}F-FPro injection. Two hours after injection of D-*cis*-^{18}F-FPro, animals were killed and the brains were removed immediately. Photographs of the whole brain were taken to document the position of the cortical infarctions, and the size of the lesions was measured. Thereafter, the brains were frozen in 2-methylbutane at −50°C and cut in coronal sections (thickness, 20 μm) with a cryostat microtome (CM 3050; Leica Mikrosysteme Vertrieb GmbH). The brain slices were placed on phosphor imaging plates (Raytest-Fuji) along with industrial ^{3}H activity standards (Microscales; Amersham Biosciences) for ^{3}H studies and with in-house calibrated ^{18}F liver paste standards. The first exposition to depict distribution of the ^{18}F radioactivity was started within 4 h after tracer injection with a duration of 14 h. This exposition was done on imaging plates that were insensitive to β-particles of ^{3}H (BAS-SR 2025; Raytest-Fuji). After decay of ^{18}F (10 half-lives), the brain slices were exposed again to ^{3}H-sensitive imaging plates for 72 h to obtain the ^{3}H distribution (BAS-TR 2025; Raytest-Fuji). On exposure, the imaging plates were scanned with a high-performance imaging plate reader (BAS 5000 BioImage Analyzer; Raytest-Fuji). Quantitative autoradiograms were generated (Bq/mg wet weight of the tissue) using the software provided by the manufacturer and the known radioactivity concentrations of the standards. Tracer uptake was quantified by lesion-to-brain ratios (L/B ratios) using a small circular region of interest (ROI) placed on an area with maximal tracer accumulation—that is, either in the area of the infarction or in the TN with increased tracer uptake (ROI, 0.2–0.5 mm^2). A larger reference ROI was placed in the contralateral hemisphere in the normal gray matter (ROI, 5–10 mm^2). L/B ratios were calculated by dividing the average uptake in the ROI of the lesion by the average uptake in the ROI of the normal brain.

Double Immunofluorescence Labeling and Histologic Staining

Double immunofluorescence labeling was performed to identify specific subtypes of cells involved in the process of tracer uptake. Reactive astrocytes were detected by staining for GFAP

TABLE 1
Summary of Data on Animals with Cortical Infarctions

Rat no.	Time after PT (d)	Cortical area	D-*cis*-FPro uptake: Thalamic nucleus, striatum	D-*cis*-FPro uptake: PT/brain	D-*cis*-FPro uptake: TN/brain	^{3}H-DG: PT/brain	^{3}H-DG: TN/brain	^{3}H-PK11195: PT/brain	^{3}H-PK11195: TN/brain	^{3}H-MET: PT/brain	^{3}H-MET: TN/brain
1	7	Mot, Sens	CPu, Po, VPM, VPL	12.6	4.0						
2	5	Mot, Sens	CPu, Po, VL	11.7	6.3	4.2	1.4				
3	8	Vis	DLG, LP	16.6	8.0	2.4	1.0				
4	7	Sens, Vis	Po, VPM, DLG	12.4	6.0	5.5	1.0				
5	7	Vis	DLG, LP	17.6	3.4	2.2	1.1				
6	7	Mot, Sens	CPu, Po, VPM, VPL, VL	9.4	4,0	3.0	1.2				
7	7	Mot	CPu, VL	16.8	4.8	3.0	1.0				
8	7	Sens	Po, VPM, VPL	10.7	9.0	2.7	0.9				
9	7	Sens	Po, VPM, VPL	6.6	5.6	2.3	0.8				
10	14	Sens	Po, VPM, VPL	31.6	11.8			5.7	1.4		
11	28	Sens	Po, VPM	4.1	9.6						
12	28	Sens	Po, VPM	24.8	13.4						
13	28	Sens	Po, VPM	7.0	9.3			8.0	1.0		
14	5	Mot, Sens	CPu, Po, VPM	11.8	3.5					2.7	1.1
15	3	Mot, Sens	CPu, Po, VPM	13.4	3.4					1.0	0.8
16	3	Mot, Sens	CPu, Po, VPM	20.8	2.4					0.6	0.9
17	2	Sens	—	3.3	—	0.9	—				
18	2	Sens	—	3.8	—	0.7	—				
19	1	Sens	—	3.4	—	1.0	—				
20	1	Sens	—	3.8	—	0.6	—				
Mean				12.1	6.7	2.5	1.0	6.8	1.2	1.4	1.0
SD				8.1	3.5	1.5	0.2	1.7	0.3	1.1	0.2

PT = cortical infarction induced by photothrombosis; ; ^{3}H-DG = ^{3}H-deoxyglucose; ^{3}H-Pk11195 = ligand for peripheral benzodiazepine receptors; ^{3}H-MET = ^{3}H-*methyl*-L-methionine; PT/brain = ratio of maximal tracer uptake PT divided by mean uptake in normal brain tissue; TN/brain = ratio of maximal tracer uptake in thalamic nucleus divided by mean uptake in normal brain; Mot = motor cortex; Sens = somatosensory cortex; CPu = caudate putamen; Po = posterior thalamic nuclear group; VPM = ventral posteromedial thalamic nucleus; VPL = ventroposterolateral thalamic nucleus; VL = ventrolateral thalamic nucleus; Vis = visual cortex; DLG = dorsal lateral geniculate nucleus; LP = lateral posterior thalamic nucleus.

using rabbit antirat GFAP polyclonal antibodies (1:1,000; abcam). Macrophages were demonstrated with mouse antirat CD68 monoclonal antibodies (1:50; Serotec), and microglia were detected with mouse antirat CD11b monoclonal antibodies (1:50; AbD Serotec). As secondary antibodies, goat antirabbit Alexa Fluor 568 or goat antimouse Alexa Fluor 488 (1:300; Invitrogen) were used. In all slices, cell nuclei were counterstained with 4′,6′-diamidino-2-phenylindole hydrochloride (2 μg/mL; Sigma-Aldrich Chemie GmbH). In addition, cell nuclei were stained histologically by toluidine blue in serial slices.

Anatomic Correlations

The position of the cortical infarctions was assessed by correlating the photographic documentation of the dorsal view of the rat brains with a stereotactic rat brain atlas (*15*). The length and width of the individual rat brains in the images were adjusted to the standard rat brain of this atlas. This adjustment allowed a rough estimation of the stereotactic coordinates of the cortical infarctions and an allocation of the infarct areas to larger functional areas, such as motor cortex, somatosensory cortex, and visual cortex.

To identify the anatomic correlates of the areas with focally increased D-*cis*-^{18}F-FPro uptake in the diencephalon, the coronal histologic slices stained by toluidine blue were compared with the anatomic maps of the stereotactic rat brain atlas. The anatomic map corresponding to the histologic slice could be identified reliably on the basis of characteristic anatomic structures. Thereafter, a circumference ROI was drawn along the borders of the coronal brain slices in the anatomic map. After adapting the size of the corresponding autoradiogram to that ROI, a small ROI was drawn at the position of focal tracer uptake in the midbrain. The set of the 2 ROIs was reprojected on the anatomic map, which allowed an identification of the TN or an area within the caudate nucleus with increased D-*cis*-^{18}F-FPro uptake (Fig. 1). All evaluations were done independently by an experienced neuroanatomist and a nuclear medicine physician and yielded identical results.

Statistical Analysis

Values are expressed as mean ± SD. The Pearson correlation coefficient was used for analysis of L/B ratios of tracer uptake at different time points after cortical infarction. A P value < 0.05 was considered significant.

RESULTS

D-*cis*-^{18}F-FPro Uptake in TN and Caudate Nucleus

Within the first 2 d after cortical infarction no pathologic uptake of D-*cis*-^{18}F-FPro was noted outside the area of the cortical infarction. From day 3 onward, focal uptake of D-*cis*-^{18}F-FPro was present in the thalamus in all animals

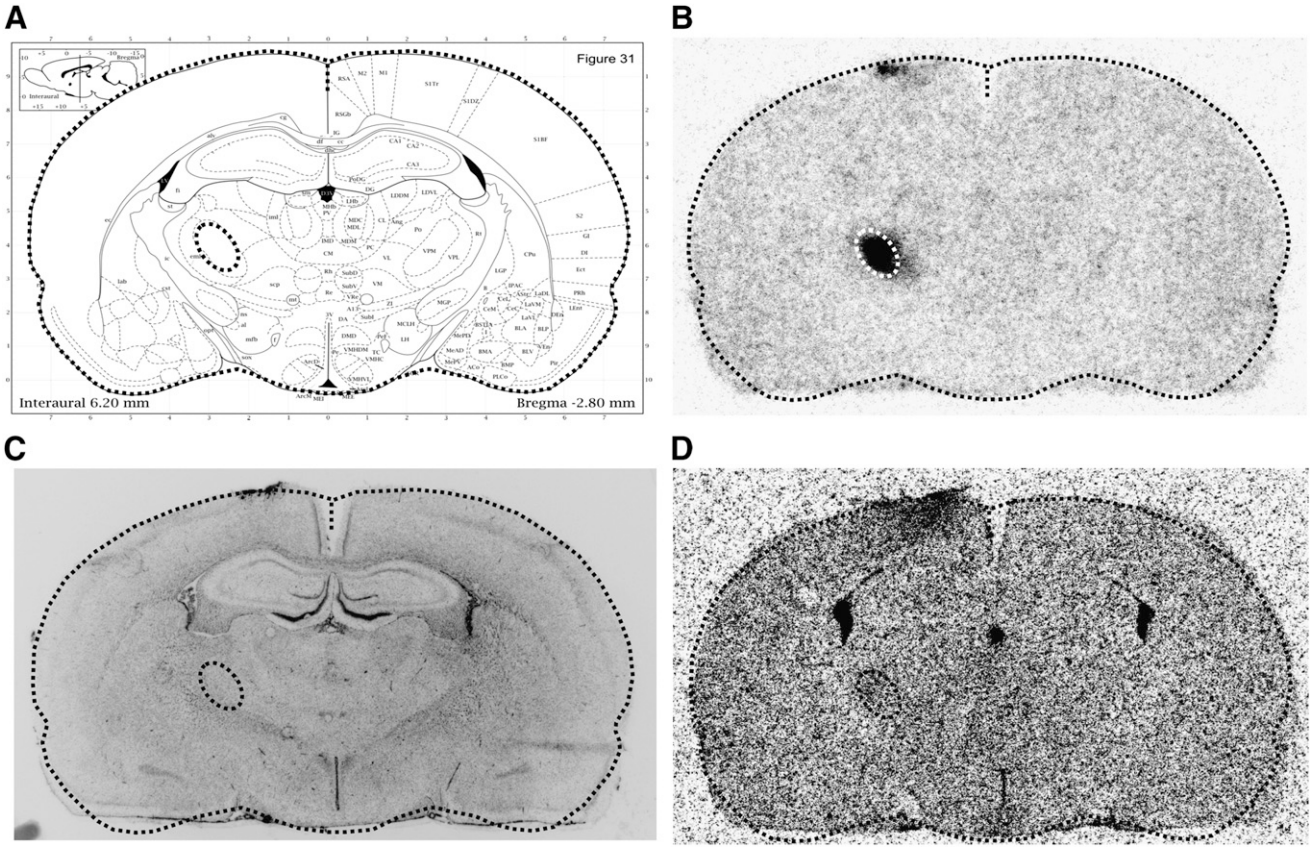

FIGURE 1. Localization of TN (rat 10): Coronal brain slice in the anatomic map (A) was identified using the histologic slice (C). The corresponding autoradiogram of D-*cis*-^{18}F-FPro (B) was adapted to the circumference of this map. Reprojection of focal tracer uptake in the midbrain to the anatomic map identifies the thalamic nucleus. The ventroposteromedial thalamic nucleus (VPM) is indicated by an ellipse. The corresponding autoradiogram using ^{3}H-PK11195 (D) shows only minor tracer uptake in the VPM. (Image A modified and reprinted with permission of (*15*).)

and partially in the corpus striatum. The thalamus or the striatum was not affected directly by the PT in any of the animals—that is, the ischemic lesions were limited strictly to the cerebral cortex. The L/B ratios of D-*cis*-^{18}F-FPro uptake in TN increased significantly with time after infarction ($r = 0.81$, $P < 0.001$, $n = 20$) (Fig. 2) (mean L/B ratio, 6.7 ± 3.5). The involved TN varied with the site of the cortical lesion—that is, only those nuclei that are sources of thalamocortical projections connecting them with their specific target region in the cerebral cortex were labeled. Thus, cortical lesions involving the motor cortex induced D-*cis*-^{18}F-FPro uptake in the ventrolateral thalamic nucleus (VL) and, additionally, in the caudate putamen (CPu); lesions in the somatosensory cortex induced D-*cis*-^{18}F-FPro uptake in the posterior thalamic nuclear group (Po), the ventroposterolateral (VPL) and ventroposteromedial TN (VPM); and lesions involving the visual cortex induced D-*cis*-^{18}F-FPro uptake in the lateral posterior thalamic nucleus (LP) and the dorsolateral geniculate nucleus (DLG). Details on the site of the cortical infarctions and the corresponding uptake in TN are given in Table 1. An example of a cortical infarction involving the motor and somatosensory cortex is shown in Figure 3 and an infarction involving the visual cortex is shown in Figure 4.

The TN with focally increased uptake of D-*cis*-^{18}F-FPro showed no major abnormalities in histologic and immunofluorescent staining up to 5 d after cortical infarction. At 7 d after infarction, TN and the caudate nucleus became weakly positive for GFAP staining in single animals (rats 6 and 8) and, from day 8 onward, the corresponding TN were positive for CD11b and GFAP staining indicating microglial activation and reactive astrocytosis (rats 3 and 10–13). Staining for CD68 antibodies in the thalamus was negative. An example is shown in Figure 5.

D-*cis*-^{18}F-FPro Uptake in Cortical Infarctions

All animals showed an increased uptake of D-*cis*-^{18}F-FPro in the area of the cortical infarctions, with L/B ratios ranging from 3.3 to 31.6 (mean L/B, 12.1 ± 8.1) (Table 1). There was no significant correlation between maximal D-*cis*-^{18}F-FPro uptake within the infarct area and the time point after induction of the PT ($r = 0.22$, $P = 0.35$, $n = 20$). Within the first 3 d after infarction, focally increased D-*cis*-^{18}F-FPro was noted in the core of the infarction and

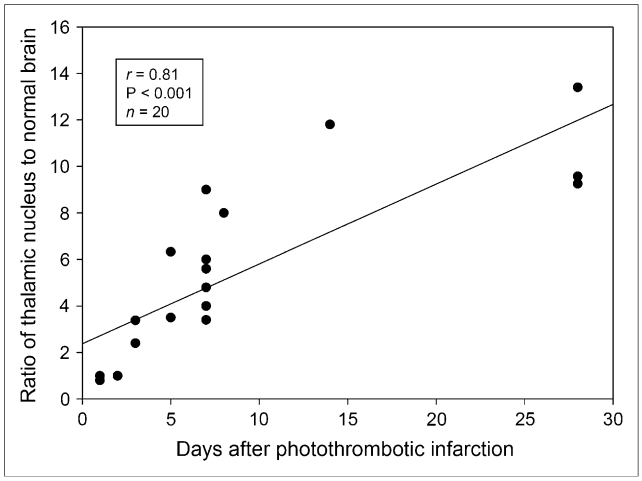

FIGURE 2. D-*cis*-^{18}F-FPro uptake in TN (ratio of tracer uptake in thalamic tissue divided by normal brain tissue) vs. time after cortical infarction. There is a significant correlation.

spots of activated microglia were present. From day 5 onward, the pattern of D-*cis*-^{18}F-FPro uptake within the infarct area was similar to that of immunostaining for CD68 and CD11b, indicating a relationship of tracer uptake to macrophage infiltration or activated microglia. There was no D-*cis*-^{18}F-FPro uptake in the rim of the infarctions, which was positive for GFAP, indicating that tracer uptake is not associated with reactive astrogliosis. An example of D-*cis*-^{18}F-FPro and ^{3}H-DG distribution in comparison with immunofluorescence staining for CD68, CD11b, and GFAP in the cortical infarction of animal 6 is shown in Figure 6.

Comparison of ^{3}H-DG, ^{3}H-L-MET, and ^{3}H-PK11195

No uptake of ^{3}H-DG or ^{3}H-L-MET was noted in TN or the caudate nucleus that showed significant D-*cis*-^{18}F-FPro uptake. ^{3}H-PK11195, which has been reported to accumulate in TN after cortical infarction (*13,14*), showed only weak tracer accumulation in the TN with accumulation of D-*cis*-^{18}F-FPro and immunopositivity for CD11b and GFAP (rats 10 and 13; L/B, 11.8 and 9.3, respectively; Fig. 1).

The cortical infarctions did not display any uptake of ^{3}H-DG within the first 2 d after PT (animals 17–20), whereas D-*cis*-^{18}F-FPro was increased. At 7 d after infarction, uptake of ^{3}H-DG was also increased (mean L/B ratio, 2.5 ± 1.5). The pattern of uptake within the infarct area was similar to that of D-*cis*-^{18}F-FPro uptake and immunostaining for CD68 and CD11b (Fig. 6). In addition, the uptake of ^{3}H-L-MET was investigated in 3 animals but revealed only weak signal within the infarct area in 1 animal.

DISCUSSION

In this study we investigated the cerebral uptake of D-*cis*-^{18}F-FPro in rats after focal cortical ischemic lesions. We found unexpected uptake of the tracer in TN and the caudate nucleus, indicating that D-*cis*-^{18}F-FPro may be a sensitive tracer for detection of secondary changes in areas remote from the primary lesion. All photothrombotic lesions were limited to the cerebral cortex, and the thalamus or caudate nucleus was not affected directly by the infarcted area in any of the animals.

D-*cis*-^{18}F-FPro Uptake in TN and Caudate Nucleus

The phenomenon of thalamic retrograde degeneration after cortical injury has been exploited effectively in classical neuroanatomic studies as a method for characterizing patterns of thalamocortical connections using Nissl stains (*16*). Thalamic neurons are characterized by a marked sensitivity to neocortical injury, resulting in rapid degeneration that effectively precludes axonal regeneration (*16,17*). Experimental studies suggest that thalamic atrophy results primarily from retrograde degeneration, due to injury of the thalamocortical pathway (*18–20*). Thalamic degeneration is associated with a prominent reaction of microglia and astrocytes that has been considered to play an active role in delayed degeneration (*21*). Cortical ablation also results in a marked decrease in thalamic high-affinity uptake of glutamate and aspartate (*16*). The failure of mechanisms removing excitatory amino acids from the milieu of affected thalamic relay neurons has been reported as a driving force in the process of thalamic retrograde degeneration. Retrograde degeneration does not occur elsewhere in the brain, even though other neural structures innervate the cerebral cortex. This suggests that thalamic neurons are particularly vulnerable (*19*).

The TN and caudate nucleus exhibiting pathologic D-*cis*-^{18}F-FPro were related to their cortical projection areas—that is, cortical lesions involving the motor cortex induced D-*cis*-^{18}F-FPro uptake in the VL and CPu, lesions in the somatosensory cortex caused uptake in the Po, VPL, and VPM, and lesions involving the visual cortex induced D-*cis*-^{18}F-FPro uptake in the LP and DLG (*22*). This finding proves that increased D-*cis*-^{18}F-FPro in TN is related to the phenomenon of thalamic retrograde degeneration. To the best of our knowledge, retrograde degeneration of the caudate nucleus after cortical infarction has not yet been described, but tracer uptake in the CPu after infarctions in the motor cortex underlines the high sensitivity of this tracer for detection of secondary changes in remote areas.

The TN with focally increased uptake of D-*cis*-^{18}F-FPro showed no major abnormalities in histologic and immunofluorescent staining up to 5 d after cortical infarction. Others have observed GFAP-positive reactive astrocytes and activated microglia already at 3 d after trauma before apoptotic cell death was detectable (*21*). D-*cis*-^{18}F-FPro uptake was clearly positive at 3 d after infarction, with L/B ratios of 2.4 and 3.5, indicating that it is a very sensitive tracer for detection of secondary changes. At 7 d after infarction, TN and the caudate nucleus became weakly positive for GFAP staining in single animals and, from day 8 onward, the corresponding TN were positive for CD11b and GFAP staining, indicating microglial activation and astrocytosis.

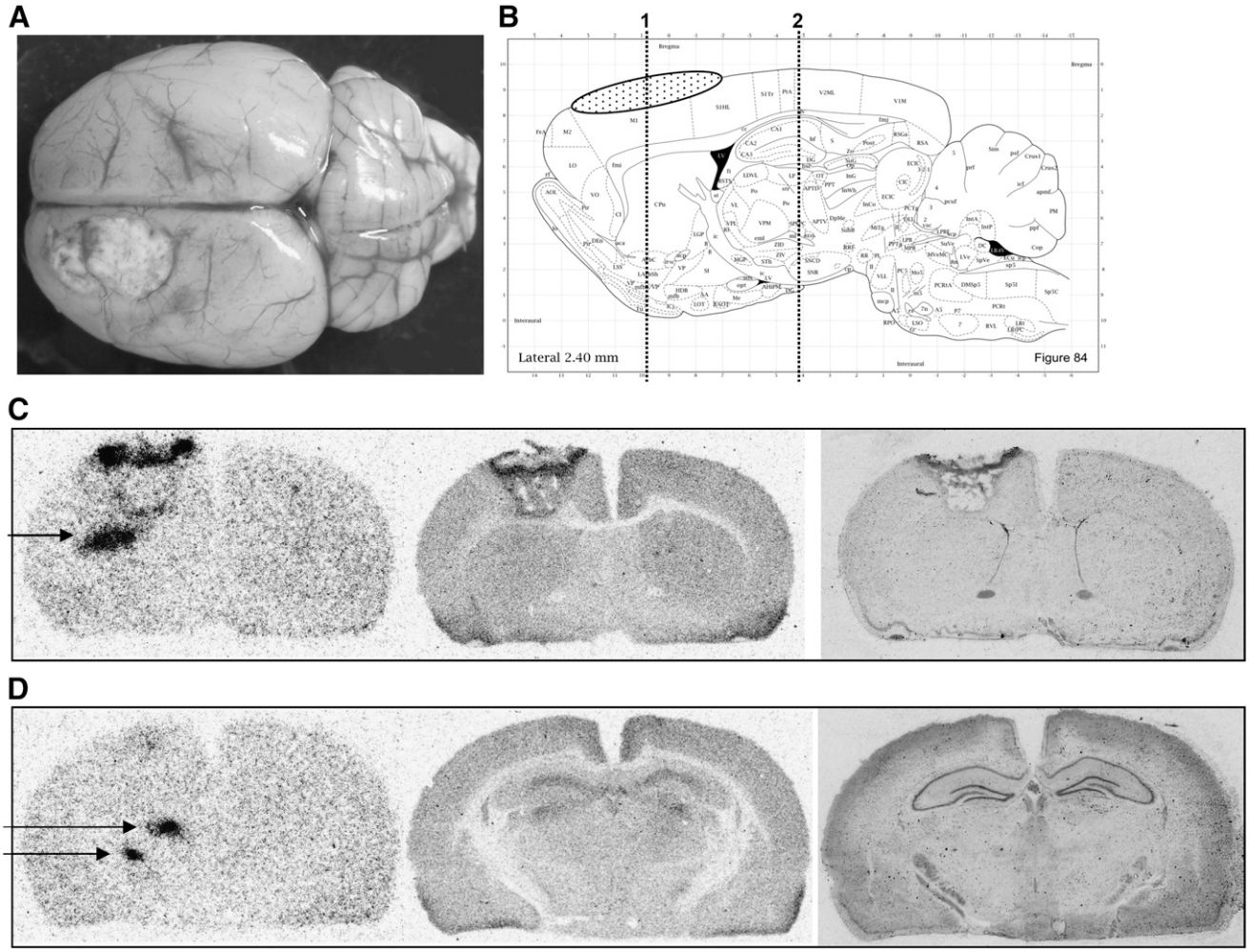

FIGURE 3. (A) Dorsal view of rat brain 7 d after PT (rat 6). Cortical infarction involves parts of motor and somatosensory cortex. (B) Sagittal slice from anatomic rat brain atlas demonstrates position of infarction (stippled area) and position of coronal slices: 1, level of basal ganglia (C); 2, level of hippocampus/thalamus (D). Autoradiogram with D-*cis*-^{18}F-FPro (C, left image) exhibits tracer uptake in area of cortical infarction and in caudate nucleus (arrow). Furthermore, there is focal D-*cis*-^{18}F-FPro uptake in ventral posteromedial thalamic nucleus and posterior thalamic nuclear group (D, left image, arrows). Corresponding autoradiograms using ^{3}H-DG (C and D, middle images) and histologic staining using toluidine blue (C and D, right images) show no abnormalities in caudate nucleus and in thalamus. (Image B modified and reprinted with permission of (*15*).)

D-*cis*-^{18}F-FPro Uptake in Cortical Infarction

The cellular components observed in our experiments are similar to those described previously in the PT model in several studies (*12,23*). Macrophages are located in a ring-like fashion around the core in the first week and later infiltrate the center of the lesion to remove debris (*24*). In all animals, we observed increased uptake of D-*cis*-^{18}F-FPro in the area of the cortical infarction. Within the first 3 d after infarction, focally increased D-*cis*-^{18}F-FPro was noted in the core of the infarction, whereas uptake of ^{3}H-DG and ^{3}H-L-MET was low. Immunofluorescence staining showed some spots of activated microglia only.

From day 5 onward, the pattern of D-*cis*-^{18}F-FPro uptake was congruent with that of immunostaining for CD11b and CD68 and with increased ^{3}H-DG uptake, indicating a relationship of tracer uptake to activated microglia and macrophage infiltration (Fig. 6). The determination of the origin of the phagocytes is difficult as microglia, the resident macrophages of the brain, are activated after ischemia and then become indistinguishable from hematogenous macrophages on morphologic grounds and based on the expression of immunocytochemical markers (*23*). However, experiments with macrophage-depleted rats have shown that, in the initial days after photochemically induced infarction, phagocytes at the border zone were primarily derived from resident microglia, whereas macrophages from the bloodstream were recruited with a delay. A pilot experiment in a rat with a bacterial abscess in the calf showed no D-*cis*-^{18}F-FPro uptake in the abscess, which was positive for CD68 staining and showed increased ^{3}H-DG

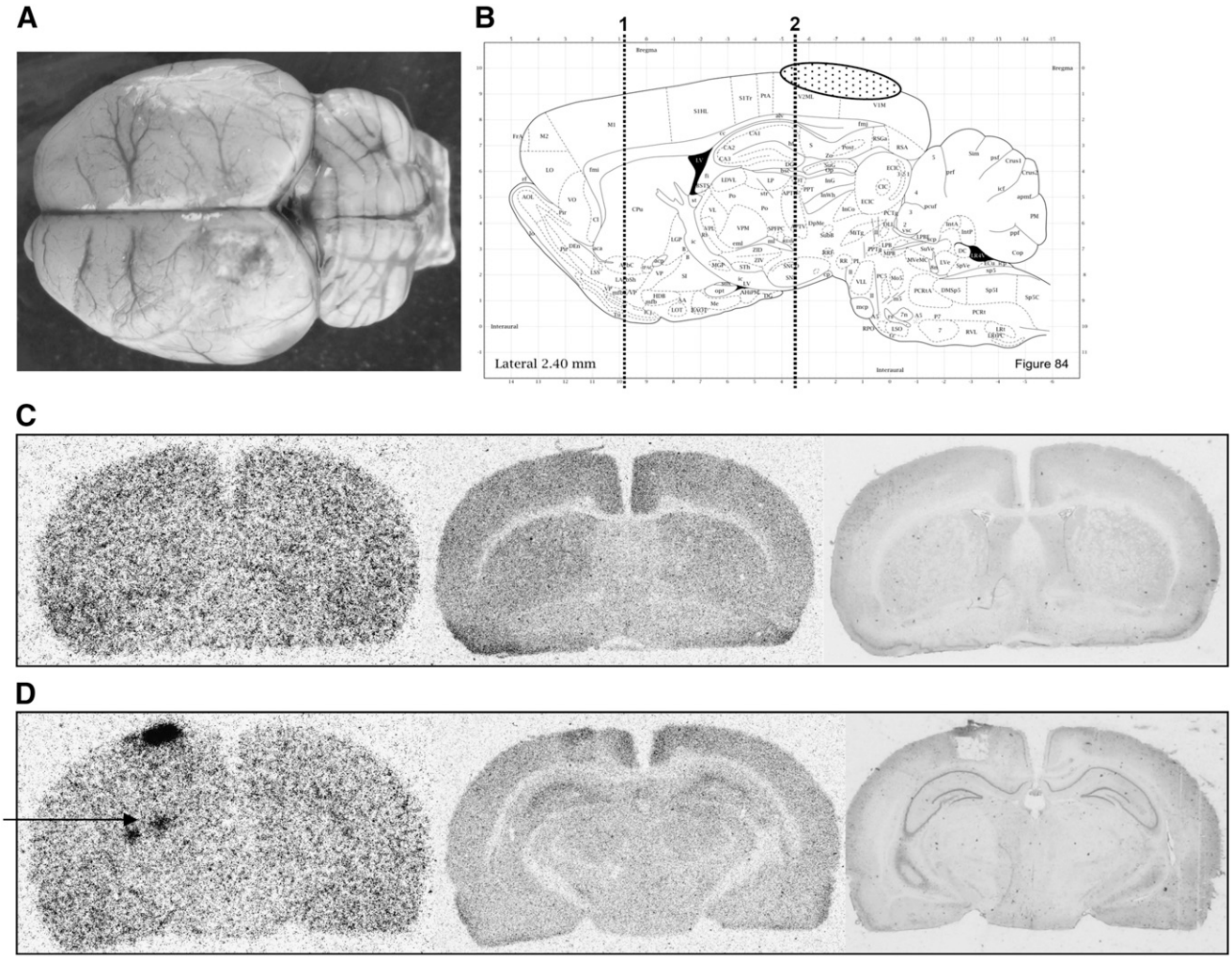

FIGURE 4. (A) Dorsal view of rat brain 7 d after PT (rat 5) with infarction in visual cortex. (B) Sagittal slice from anatomic rat brain atlas demonstrates position of infarction (stippled area) and position of coronal slices: 1, level of the basal ganglia (C); 2, level of the hippocampus/thalamus (D). Autoradiograms with D-*cis*-^{18}F-FPro (C and D, left images) exhibit tracer uptake in area of cortical infarction and in lateral posterior thalamic nucleus (LP) and dorsolateral geniculate nucleus (DLG) (D, arrow). Corresponding autoradiograms using ^{3}H-DG (C and D, middle images) and histologic staining using toluidine blue (C and D, right images) show no abnormalities in thalamus. (Image B modified and reprinted with permission of (*15*).)

uptake (data not shown). Also, the TN with increased D-*cis*-^{18}F-FPro uptake were negative for CD68 staining, so that tracer uptake in blood-borne macrophages is unlikely.

Reactive astrogliosis with upregulation of GFAP develops after 3 d in the boundary zone of photothrombotic lesions and ends up in the scar formation in the atrophic stage at day 60 (*25*). D-*cis*-^{18}F-FPro showed no uptake in the areas that were positive for GFAP staining, thus indicating that tracer uptake is not associated with reactive gliosis (Fig. 6). Because we did not evaluate the influence of BBB disruption on tracer uptake, it cannot be excluded that radioactivity within the infarct area was influenced by passive diffusion of the tracer or its metabolites. D-*cis*-^{18}F-FPro, however, is able to penetrate the intact BBB and a disruption of the BBB is not a prerequisite for tracer accumulation (*7*).

In summary, D-*cis*-^{18}F-FPro uptake in the infarct region is similar to activated microglia and phagocyte activity but is not similar to reactive astrogliosis. Because uptake in blood-borne macrophages is low, D-*cis*-^{18}F-FPro uptake appears to be related primarily to activated microglia.

Imaging Thalamic Degeneration with MRI and PET

The phenomenon of retrograde thalamic degeneration is known from experimental and pathologic investigations but also has been observed with modern imaging methods. MRI after cerebral infarction in the territory of the middle cerebral artery demonstrated secondary degeneration in the ventral nuclei of the thalamus as regions of slightly low signal on proton-density or T2-weighted images, primarily obtained a few weeks after the onset (*26*). An area of

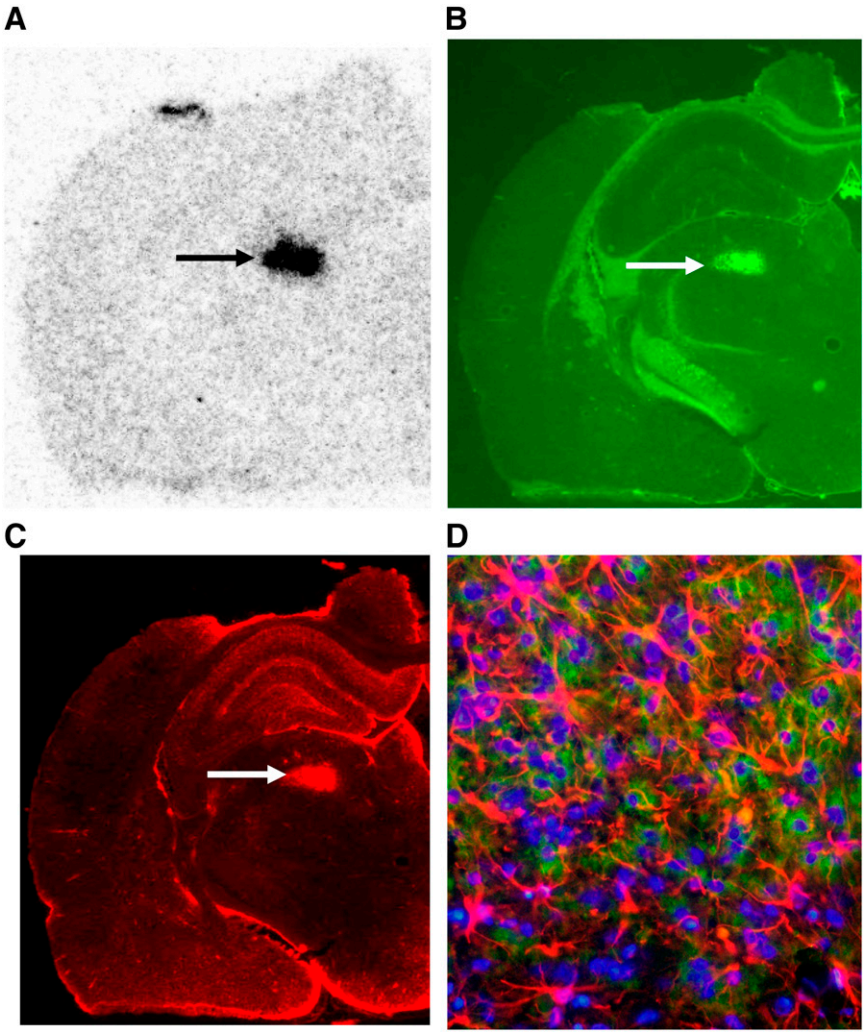

FIGURE 5. (A–C) Coronal slices of left hemisphere at level of thalamus 28 d after PT (rat 11). (A) Autoradiogram using D-*cis*-^{18}F-FPro shows high uptake in posterior thalamic nuclear group (arrow). (B) Immunofluorescent staining using CD11b shows activated microglia (arrow). (C) Immunofluorescent staining using GFAP shows reactive astrogliosis in same area (arrow) as in B. (D) Thalamic nucleus at higher magnification: blue = cell nuclei; red = astrocytes; green = activated microglia.

slightly higher signal was observed in the dorsomedial nucleus of the thalamus on T2-weighted images about 6 wk after the onset. Similarly, hypointense areas in the ipsilateral thalamus were observed on T2-weighted spin-echo images in 47% of the patients at 1–12 mo after the stroke onset (*27*). In parallel, hypoperfusion of the ipsilateral thalamus was observed in 21 of 23 patients who underwent additional SPECT studies. MRI using diffusion tensor imaging demonstrated an increase in diffusion in the ipsilateral thalamus >1 mo after the stroke onset without parallel changes in fractional anisotropy (*28*). In some patients, this increase was preceded by a transient decrease in diffusion possibly related to an early swelling of these cells.

Using the receptor ligand ^{3}H-PK11195, which binds to peripheral-type benzodiazepine receptors, autoradiographic studies in rats after focal cortical infarctions demonstrated secondary lesions in the thalamus during the second week after lesioning. ^{3}H-PK11195 binding correlated with infiltration of macrophages in the thalamus and in the primary lesion (*13*). In our study, a comparison of D-*cis*-^{18}F-FPro binding with that of ^{3}H-PK11195 was performed in 2 animals but we found only minimal ^{3}H-PK11195 binding in the TN with prominent D-*cis*-^{18}F-FPro uptake. Therefore, the sensitivity of D-*cis*-^{18}F-FPro uptake appears to be considerably higher than that of ^{3}H-PK11195 binding. A PET study using ^{11}C-PK11195 in patients after stroke detected increased tracer binding in the thalamus ipsilateral to the stroke between 2 and 24 mo after insult (*14*).

Perspectives of PET Using D-*cis*-^{18}F-FPro

When compared with the results of other techniques, PET using D-*cis*-^{18}F-FPro may be a more sensitive technique for detection of retrograde thalamic involvement after cortical infarction. We found a strong signal already at 3 d after infarction, whereas MRI and PET using ^{11}C-PK11195 were unable to detect thalamic involvement at this stage. In contrast to ^{11}C-PK11195, which has been used in many PET studies, D-*cis*-^{18}F-FPro fulfills all requirements for widespread clinical application, including efficient radiosynthesis, ^{18}F labeling with a 109-min half-life, and suitable tracer kinetics for brain imaging (*7*).

However, D-*cis*-^{18}F-FPro stability in vivo is not optimal. The percentage of intact D-*cis*-^{18}F-FPro of total radioactivity in the plasma of humans was found to be ~85% at

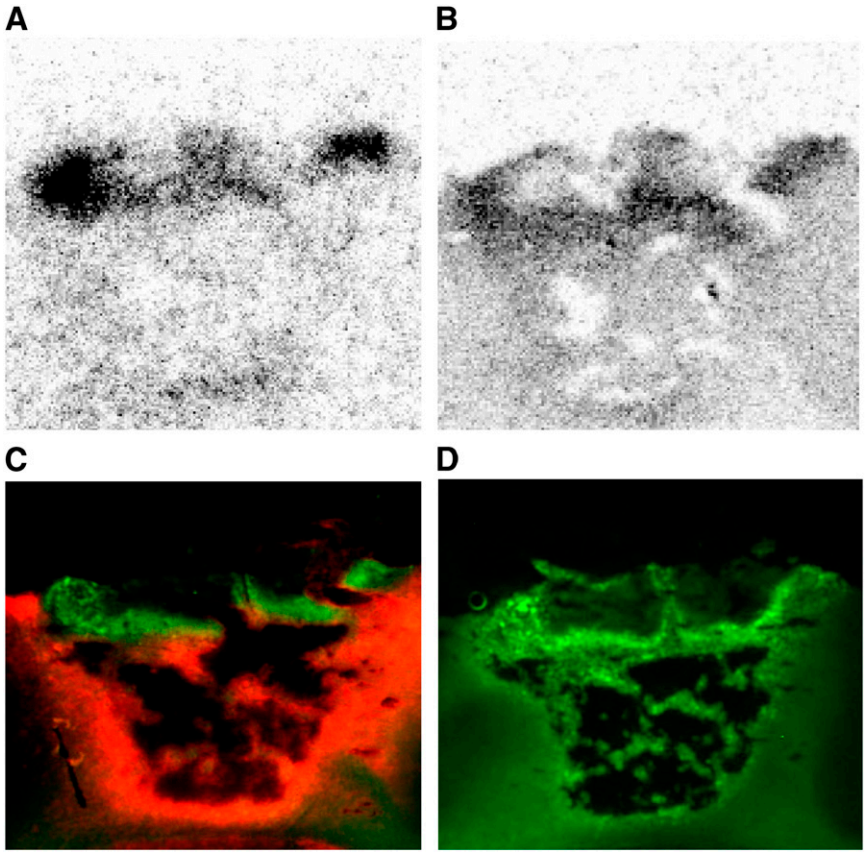

FIGURE 6. Cortical infarction 7 d after PT. (A and B) Autoradiographic distribution of D-*cis*-^{18}F-FPro (A) and ^{3}H-DG (B). (C) Double immunofluorescence labeling using CD11b shows activated microglia (green) and GFAP shows reactive astrogliosis (red). (D) Immunofluorescence labeling using CD68 shows macrophages. D-*cis*-^{18}F-FPro and ^{3}H-DG accumulation is similar to high density of activated microglia and macrophages but different from that of reactive astrocytosis.

5 min after injection, ~80% at 20 min after injection, and ~65% at 60 and 120 min after injection (*7*). Thus, some metabolic degradation of the tracer and uptake of metabolites cannot be excluded. However, analysis of the brain homogenates of rats revealed that the entire radioactivity in the brain was due to free fluoroproline, indicating that the tracer signal in the brain is not caused by metabolites (*7*). In the area of the cortical infarction, the function of the BBB may be disturbed and a penetration of metabolites cannot be excluded. In the thalamus, however, no contrast enhancement has been reported in CT and MRI studies at any stage after cortical infarction (*27*), so that a disruption of the BBB in this area can be excluded.

The nature of the amino acid carriers at the BBB, which transport the D-isomer of proline, remains to be elucidated. Recently, 2 novel mammalian amino acid cotransporters have been characterized by expression in *Xenopus* oocytes, which induce a pH-dependent electrogenic transport actvity for the small amino acids glycine, alanine, and proline (*29*). The messenger RNA of the transporter mPAT1 was highly expressed in the brain and in epithelial barriers, and the D-isomer of proline displayed a higher affinity for mPAT1 than for L-proline (*30,31*). PAT2 was expressed in neurons positive for the *N*-methyl-D-aspartate subtype of glutamate receptor subunit NR1 but not at epithelial cell membranes (*31,32*).

The possible relationship of *cis*-^{18}F-FPro uptake to microglial activation suggests an application in various brain diseases. Local activation of microglia is considered as an important process not only in classical inflammatory brain disease, such as in multiple sclerosis, but also in a variety of noninflammatory neurologic conditions, including neurodegenerative diseases, such as Alzheimer's disease and Parkinson's disease (*33*). Therefore, a further evaluation of this tracer in humans is warranted.

CONCLUSION

Our data indicate that D-*cis*-^{18}F-FPro is a sensitive PET tracer for detection of secondary degeneration of TN after cortical injury. The uptake mechanisms of D-*cis*-^{18}F-FPro remain to be elucidated, but there is some relationship to microglial activation, which suggests a promising diagnostic potential in various brain diseases.

ACKNOWLEDGMENTS

The authors thank Stefanie Klein, Markus Cremer, and Norbert Hartwigsen for assistance in animal experiments and histologic and immunofluorescent staining and Silke Grafmüller, Bettina Palm, Erika Wabbals, and Sascha Rehbein for assistance in the radiosynthesis of D-*cis*-^{18}F-FPro.

REFERENCES

1. Cohen SM, Nadler JV. Proline-induced potentiation of glutamate transmission. *Brain Res.* 1997;761:271–282.

2. Arundine M, Tymianski M. Molecular mechanisms of glutamate-dependent neurodegeneration in ischemia and traumatic brain injury. *Cell Mol Life Sci.* 2004;61:657–668.
3. Hamacher K. Synthesis of n.c.a. cis- and trans-4-[^{18}F]fluoro-L-proline, radiotracer for PET-investigation of disordered matrix protein synthesis. *J Labelled Compd Radiopharm.* 1999;42:1135–1142.
4. Wester HJ, Herz M, Senekowitsch-Schmidtke R, Schwaiger M, Stöcklin G, Hamacher K. Preclinical evaluation of 4-[^{18}F]fluoroprolines: diastereomeric effect on metabolism and uptake in mice. *Nucl Med Biol.* 1999;3:259–265.
5. Langen KJ, Börner AR, Müller-Mattheis V, et al. Uptake of cis-4-[^{18}F]-fluoro-L-proline in urologic tumors. *J Nucl Med.* 2001;42:752–754.
6. Langen KJ, Jarosch M, Hamacher K, et al. Imaging of gliomas with cis-4-[^{18}F]fluoro-L-proline. *Nucl Med Biol.* 2004;31:67–75.
7. Langen KJ, Hamacher K, Bauer D, et al. Preferred stereoselective transport of the D-isomer of cis-4-[^{18}F]fluoro-proline at the blood-brain barrier. *J Cereb Blood Flow Metab.* 2005;25:607–616.
8. Dahnke HG, Garweg G. Behavior of D- and L-proline in protein metabolism of the mouse brain and cerebellum [in German]. *Hoppe Seylers Z Physiol Chem.* 1972;353:1507.
9. Garweg G, Dahnke HG. Amino-acid racemase in the organism of mammals [in German]. *Naturwissenschaften.* 1973;60:201.
10. Garweg G, Dahnke HG. Is the conversion of D-proline into L-proline in the brain a prerequisite for the incorporation into nerve-cell proteins? *Verh Anat Ges.* 1974;68:375–379.
11. Watson BD, Dietrich WD, Busto R, et al. Induction of reproducible brain infarction by photochemically initiated thrombosis. *Ann Neurol.* 1985;17:497–504.
12. Bidmon HJ, Jancsik V, Schleicher A, et al. Structural alterations and changes in cytoskeletal proteins and proteoglycans after focal cortical ischemia. *Neuroscience.* 1998;82:397–420.
13. Myers R, Manjil LG, Frackowiak RS, Cremer JE. [^{3}H]PK 11195 and the localisation of secondary thalamic lesions following focal ischaemia in rat motor cortex. *Neurosci Lett.* 1991;133:20–24.
14. Pappata S, Levasseur M, Gunn RN, et al. Thalamic microglial activation in ischemic stroke detected in vivo by PET and [^{11}C]PK1195. *Neurology.* 2000;55:1052–1054.
15. Paxinos G, Watson C, eds. *The Rat Brain in Stereotaxic Coordinates*. 4th ed. Amsterdam, The Netherlands: Elsevier Academic Press; 1998.
16. Ross DT, Ebner FF. Thalamic retrograde degeneration following cortical injury: an excitotoxic process? *Neuroscience.* 1990;35:525–550.
17. Sorensen JC, Dalmau I, Zimmer J, Finsen B. Microglial reactions to retrograde degeneration of tracer-identified thalamic neurons after frontal sensorimotor cortex lesions in adult rats. *Exp Brain Res.* 1996;112:203–212.
18. Fujie W, Kirino T, Tomukai N, Iwasawa T, Tamura A. Progressive shrinkage of the thalamus following middle cerebral artery occlusion in rats. *Stroke.* 1990;21:1485–1488.
19. Iizuka H, Sakatani K, Young W. Neural damage in the rat thalamus after cortical infarcts. *Stroke.* 1990;21:790–794.
20. Kataoka K, Hayakawa T, Yamada K, Mushiroi T, Kuroda R, Mogami H. Neuronal network disturbance after focal ischemia in rats. *Stroke.* 1989;20:1226–1235.
21. Hermann DM, Mies G, Hata R, Hossmann KA. Microglial and astrocytic reactions prior to onset of thalamic cell death after traumatic lesion of the rat sensorimotor cortex. *Acta Neuropathol (Berl).* 2000;99:147–153.
22. Paxinos G, ed. *The Rat Nervous System*. 2nd ed. San Diego, CA: Academic Press; 2004.
23. Stoll G, Jander S, Schroeter M. Inflammation and glial responses in ischemic brain lesions. *Prog Neurobiol.* 1998;56:149–171.
24. Jander S, Kraemer M, Schroeter M, et al. Lymphocytic infiltration and expression of intercellular adhesion molecule-1 in photochemically induced ischemia of the rat cortex. *J Cereb Blood Flow Metab.* 1995;15:42–45.
25. Schroeter M, Schiene K, Kraemer M, et al. Astroglial responses in photochemically induced focal ischemia of the rat cortex. *Exp Brain Res.* 1995;106:1–6.
26. Nakane M, Tamura A, Sasaki Y, Teraoka A. MRI of secondary changes in the thalamus following a cerebral infarct. *Neuroradiology.* 2002;44:915–920.
27. Ogawa T, Yoshida Y, Okudera T, Noguchi K, Kado H, Uemura K. Secondary thalamic degeneration after cerebral infarction in the middle cerebral artery distribution: evaluation with MR imaging. *Radiology.* 1997;204:255–262.
28. Herve D, Molko N, Pappata S, et al. Longitudinal thalamic diffusion changes after middle cerebral artery infarcts. *J Neurol Neurosurg Psychiatry.* 2005;76:200–205.
29. Boll M, Foltz M, Rubio-Aliaga I, Kottra G, Daniel H. Functional characterization of two novel mammalian electrogenic proton-dependent amino acid cotransporters. *J Biol Chem.* 2002;277:22966–22973.
30. Metzner L, Neubert K, Brandsch M. Substrate specificity of the amino acid transporter PAT1. *Amino Acids.* 2006;31:111–117.
31. Brandsch M. Transport of L-proline, L-proline-containing peptides and related drugs at mammalian epithelial cell membranes. *Amino Acids.* 2006;31:119–136.
32. Rubio-Aliaga I, Boll M, Vogt-Weisenhorn DM, Foltz M, Kottra G, Daniel H. The proton/amino acid cotransporter PAT2 is expressed in neurons with a different subcellular localization than its paralog PAT1. *J Biol Chem.* 2004;279:2754–2760.
33. Banati RB. Visualising microglial activation in vivo. *Glia.* 2002;40:206–217.